

Submitted: February 2, 2008

The Rich Mid-Infrared Environments of Two Highly-Obscured X-ray Binaries: *SPITZER* Observations of IGR J16318–4848 and GX 301–2

Dae-Sik Moon¹, David L. Kaplan², William T. Reach³, Fiona A. Harrison⁴, Jeong-Eun Lee⁵, Peter G. Martin⁶

ABSTRACT

We present the results of *SPITZER* mid-infrared spectroscopic observations of two highly-obscured massive X-ray binaries: IGR J16318–4848 and GX 301–2. Our observations reveal for the first time the extremely rich mid-infrared environments of this type of source, including multiple continuum emission components (a hot component with $T > 700$ K and a warm component with $T \sim 180$ K) with apparent silicate absorption features, numerous H I recombination lines, many forbidden ionic lines of low ionization potentials, and pure rotational H₂ lines. This indicates that both sources have hot and warm circumstellar dust, ionized stellar winds, extended low-density ionized regions, and photo-dissociated regions. It appears difficult to attribute the total optical extinction of both sources to the hot and warm dust components, which suggests that there could be an otherwise observable colder dust component responsible for the most of the optical extinction and silicate absorption features. The observed mid-infrared spectra are similar to those from Luminous Blue Variables, indicating

¹Department of Astronomy and Astrophysics, University of Toronto, Toronto, ON M5S 3H4, Canada; moon@astro.utoronto.ca

²Pappalardo Fellow, Kavli Institute for Astrophysics & Space Research and Department of Physics, Massachusetts Institute of Technology, Cambridge, MA 02139; dlk@space.mit.edu

³Infrared Processing Analysis Center, California Institute of Technology, MS 220-6, Pasadena, CA 91125; reach@ipac.caltech.edu

⁴Space Radiation Laboratory, California Institute of Technology, MC 220-47, Pasadena, CA 91125; fiona@srl.caltech.edu

⁵Department of Astronomy and Space Science, Sejong University, Seoul 143-747, Korea; jelee@sejong.ac.kr

⁶Canadian Institute for Theoretical Astrophysics, University of Toronto, Toronto, ON M5S 3H8, Canada; pgmartin@cita.utoronto.ca

that the highly-obscured massive X-ray binaries may represent a previously unknown evolutionary phase of X-ray binaries with early-type optical companions. Our results highlight the importance and utility of mid-infrared spectroscopy to investigate highly-obscured X-ray binaries.

Subject headings: circumstellar matter — infrared: stars — stars: emission-line, Be — X-rays: binaries — X-rays: individual (GX 301–2, IGR J16318–4848)

1. Introduction

Recently, a large number of highly-obscured (e.g., $N_{\text{H}} \geq 10^{23} \text{ cm}^{-2}$) massive X-ray binaries have been discovered by the *INTEGRAL* hard X-ray ($\geq 15 \text{ keV}$) satellite (Winkler et al. 2003). The prototypical case is IGR J16318–4848 which shows variable high obscuration in the X-ray, sometimes reaching $N_{\text{H}} \simeq 2 \times 10^{24}$ (Courvoisier et al. 2003; Walter et al. 2003). Its bright optical and near-infrared (IR) counterpart is an early B-type supergiant star with numerous emission lines (Filliatre & Chaty 2004). Interestingly the obscuration toward IGR J16318–4848 obtained in the optical and near-IR wavebands ($A_{\text{V}} \sim 18$) is almost two orders of magnitude smaller than that inferred from the X-rays, which suggests that the extreme obscuration seen in the X-ray is intrinsic only to the X-ray source. However, $A_{\text{V}} \sim 18$ is still greater than the interstellar obscuration, indicating the existence of substantial circumstellar material around the supergiant companion.

In order to fully understand the implications of the *INTEGRAL* discoveries — specifically if they imply existence of a separate class of highly-obscured X-ray binaries — we must investigate any similarities between the new *INTEGRAL* sources and previously known sources. As already suggested by Revnivtsev et al. (2003), the X-ray pulsar GX 301–2 appears similar to the new *INTEGRAL* highly-obscured massive X-ray binaries: it has variable X-ray obscuration of $N_{\text{H}} \simeq 10^{23}\text{--}10^{24} \text{ cm}^{-2}$, the compact source is a neutron star, and the optical companion is an early B-type supergiant (or hypergiant; Kaper et al. 1995), like IGR J16318–4848. Recently, Kaplan, Moon, & Reach (2006, ; hereafter Paper I), using optical, near-, and mid-IR ($\leq 20 \text{ }\mu\text{m}$) spectral energy distributions (SEDs), have found that both sources have strong mid-IR excesses that they identify as continuum emission from hot dust. This is suggestive that they have very similar circumstellar material which may be related to their strong X-ray obscuration. In this *Letter*, we present the results of *SPITZER* mid-IR spectroscopic observations of IGR J16318–4848 and GX 301–2, showing that both sources indeed have very similar rich mid-IR properties previously unknown for X-ray binaries.

2. Observations and Data Reduction

We observed IGR J16318–4848 and GX 301–2 with *InfraRed Spectrograph* (IRS) aboard *SPITZER* (Houck et al. 2004; Werner et al. 2004) on 2005 September 8 and 2005 July 2, respectively. The duration of the total observations was 1.32 (IGR J16318–4848) and 0.82 (GX 301–2) hours with the all six IRS modules in operation in the standard staring mode, obtaining two nods of spectra separated by $1/3$ of the slit length. For the basic data reduction, we used the co-added Basic Calibration Data (BCD) produced through the standard *SPITZER* Science Center data reduction pipeline (S13.2.0), and also the *SPITZER* IRS Custom Extraction (i.e., SPICE) software (v1.3-beta1). In the low-resolution mode where the slit lengths are large (i.e., $57''$ for $5.2\text{--}14.5\text{ }\mu\text{m}$ and $168''$ for $14.0\text{--}38.0\text{ }\mu\text{m}$), we subtracted out background emission of one nod using the spectrum of the another nod, and combined the two background-subtracted spectra for the final spectrum. However, in the high-resolution mode, the small slit length (i.e., $11''.3$ for $9.9\text{--}19.6\text{ }\mu\text{m}$ and $22''.3$ for $18.7\text{--}37.2\text{ }\mu\text{m}$), together with the high brightnesses of the sources, made it impossible to subtract out the background. Therefore, we just combined the spectra from the two nods for the final high-resolution spectrum without any background subtraction. In addition, we used IRSCLEAN (v1.5) to mask and clean rogue pixels from the co-added BCD images, and then interpolated over neighboring normal pixels.

3. Low-Resolution Spectrum: Continuum and Broad Features

Some emission features, such as ionic forbidden lines, H_2 lines, and Polycyclic Aromatic Hydrocarbon (PAH) emission, present in the low-resolution spectra appear extended. Here we consider just the emission from point sources, and defer discussion of the extended emission to a separate paper. Figure 1 presents the background-subtracted low-resolution spectrum of IGR J16318–4848, as well as the best-fit spectra of the continuum emission and the residual of the SED fit (see below). Note that the low-resolution spectrum is extracted for the continuum source (i.e., IGR J16318–4848) based on the standard point source extraction procedure of SPICE. Several features are prominent in Figure 1, including complicated multi-component continuum emission, broad and strong absorption around 9.7 and $18\text{ }\mu\text{m}$, and numerous emission lines. The spectrum of GX 301–2 (Figure 2) is similar, with strong continuum emission, silicate absorptions feature around $9.7\text{ }\mu\text{m}$, and several emission lines.

As in Figures 1 and 2, the silicate absorption features and numerous emission lines make it difficult to carry out any meaningful independent SED fits of the shorter wavelength (i.e., $\lambda \leq 8\text{ }\mu\text{m}$) data of the IRS spectra. Therefore, instead, we first examined if the IRS SEDs at the shorter wavelengths are consistent with what have been found in Paper I using

only the line-free regions. According to Paper I, the SEDs of IGR J16318–4848 and GX 301–2 at $\lambda \leq 8 \mu\text{m}$ have contributions from hot (i.e., $T \simeq 1040 \text{ K}$ for IGR J16318–4848 and 720 K for GX 301–2) dust emission and stellar emission of a B0I star with temperature of 26000 K , while the contribution of free-free emission is negligible. Our IRS SEDs of the line-free regions in Figures 1 and 2 at $\lambda \leq 8 \mu\text{m}$ were fitted very well with those parameters, resulting in the reduced chi-square $\chi^2_\nu \leq 1$. We used the extinction $A_V = 18.5$ and 7.1 for IGR J16318–4848 and GX 301–2, respectively, as in Paper I. However, in the longer wavelength (i.e., $\lambda \geq 22 \mu\text{m}$) range, we were unable to fit the IRS SEDs with the given hot dust and stellar parameters because the best fit resulted in unacceptably large chi-square values. We therefore performed SED fits with three components (i.e., hot dust, stellar, and warm dust component) using the entire line-free SEDs in the $\lambda \leq 8 \mu\text{m}$ and $\geq 22 \mu\text{m}$ range. Over the fits the parameters of the warm dust component were treated as free parameters, while those of the hot dust and stellar component were fixed to be the values in Paper I. As a result, we obtained the warm dust temperature of 190 K (IGR J16318–4848) and 170 K (GX 301–2) with $\chi^2_\nu \simeq 1.2$ (IGR J16318–4848) and 1.5 (GX 301–2). We used the extinction coefficients compiled in Mathis (2000) excluding the $8\text{--}22 \mu\text{m}$ range in order to avoid the uncertainties of the coefficients associated with the silicate absorption features. We instead interpolated the extinction coefficients at $\lambda \leq 8$ and $\geq 22 \mu\text{m}$ to calculate the silicate absorption-free extinction coefficients in the $\lambda = 8\text{--}22 \mu\text{m}$ range, and used them in the fits. The main panel of Figures 1 and 2 presents the results of our best SED fit obtained by excluding the silicate absorption features, where we can confirm that the fit matches nicely the observed SED except the $\lambda = 8\text{--}22 \mu\text{m}$ range. In the bottom panel, on the other hand, we show the residuals of the fit obtained by subtracting the fluxes computed by the best fit from the observed values. For this residual construction, in order to see if our best SED fit is consistent with the observed silicate absorption features, we combined the best-fit parameters obtained at $\lambda \leq 8$ and $\geq 22 \mu\text{m}$ with the extinction coefficients in the $\lambda = 8\text{--}22 \mu\text{m}$ range (Mathis 2000), and calculated the silicate absorption feature-associated fluxes expected by the best SED fit in the $\lambda = 8\text{--}22 \mu\text{m}$ range. The residuals in Figures 1 and 2 show that overall our best SED fit agrees with the silicate absorption features reasonably well, although there appears to be some small discrepancies for IGR J16318–4848.

The masses of the dust components were estimated under the optically thin assumption (Hildebrand et al. 1977): $M_{\text{dust}} = F_\lambda d^2 / \kappa_\lambda B_\lambda(T_{\text{dust}})$, where d is the distance to the source, κ_λ is the dust mass absorption coefficient, and $B_\lambda(T)$ is the Planck function at temperature T . Using the interstellar mass absorption coefficients of Draine (2003) at 8 and $25 \mu\text{m}$, the hot and warm dust masses are estimated to be $M_{\text{hot}} \simeq 4.5 \times 10^{-9} d_5^2 M_\odot$ and $M_{\text{warm}} \simeq 3.1 \times 10^{-7} d_5^2 M_\odot$ for IGR J16318–4848; $M_{\text{hot}} \simeq 5.7 \times 10^{-9} d_5^2 M_\odot$ and $M_{\text{warm}} \simeq 1.4 \times 10^{-7} d_5^2 M_\odot$ for GX 301–2, where d_5 is the distance to the sources normalized by 5 kpc .

The silicate absorption features seen in Figures 1 and 2 have a tight linear correlation with the optical extinction in the diffuse interstellar medium (ISM), although the correlation has been reported to break down in dense environment where the silicate feature does not show a monotonic increase with extinction at $A_V \geq 12$ mag (e.g., Chiar et al. 2007, and references therein). The correlation in the diffuse ISM is $A_V/\tau_{9.7} = 18.5$ (Draine 2003, and references therein; $\tau_{9.7}$ is the optical depth of the silicate absorption at $9.7 \mu\text{m}$). If we adopt the above correlation given in the diffuse ISM, the intensity ratio of the observed spectrum to the unabsorbed spectrum in Figures 1 and 2 at $9.7 \mu\text{m}$ correspond to $A_V \sim 18.5$ and ~ 6 for IGR J16318–4848 and GX 301–2, respectively. These are very similar to the values obtained in previous studies for the total optical extinctions of the both sources. This suggests that a substantial portion, if not all, of the silicate features seen in Figures 1 and 2 are associated with the optical extinction of IGR J16318–4848 and GX 301–2.

4. High-Resolution Spectrum: Line Emission

Figures 3 and 4 present high-resolution spectrum of IGR J16318–4848 and GX 301–2, revealing numerous emission lines. (Note that the background emission is *NOT* subtracted.) The majority of them are H I lines, while the rest consists of metallic forbidden lines, pure rotational H_2 lines, and $11.3 \mu\text{m}$ PAH emission feature. Table 1 lists the intensities of some of the bright H I lines identified in both sources with high (> 3) signal-to-noise ratio. The line intensities and the signal-to-noise ratio were estimated with Gaussian profile fits. The intensities of the H I lines are consistent with gas at $T \simeq 10^4$ K and with $N_e \simeq 10^4 \text{ cm}^{-3}$ in the Menzel Case B state, following Filliatre & Chaty (2004), although the intensity ratios are not very sensitive to those parameters (Hummer & Storey 1987).

Table 2 lists the parameters of forbidden ionic lines and H_2 lines. For the forbidden lines, [Ne II], [Ne III], [S III], and [Si II] were detected in both sources, while [Ni II] and [Fe II] were only in IGR J16318–4848; [Fe III] is only in GX 301–2. The H_2 lines were detected in both sources. The intensity ratio of the [S III] lines of 18.7 and $33.5 \mu\text{m}$ is diagnostic of the number density in the temperature range of 5000 – 20000 K. The extinction-corrected [S III] line surface brightness ratio of $18.7/33.5 \mu\text{m}$ is 1.21 for IGR J16318–4848 and 1.68 for GX 301–2: according to the calculation of Houck et al. (1984) and Alexander et al. (1999), the ratios correspond to the electron number density $N_e \sim 1000 \text{ cm}^{-3}$ for both sources. On the other hand, the intensity ratio of the [Ne II] line ($12.8 \mu\text{m}$) and the [Ne III] line ($15.6 \mu\text{m}$) is sensitive to the hardness of the radiation, or temperature of the environment. If we use the calculation of Kunze et al. (1996), the extinction-corrected intensity ratio of [Ne II]/[Ne III] is consistent with $\sim 4 \times 10^4$ K for IGR J16318–4848 and $\sim 4.5 \times 10^4$ K for GX

301–2. The three H_2 lines detected in the both sources are pure rotational transition lines of H_2 (0,0) S(0,1,2) which are usually excited by collisions. Assuming that the bottom two lines follow the distribution of the local thermodynamic equilibrium and are optically thin, the surface brightness ratios are consistent with the excitation temperature $T_{\text{ex}} \sim 1000$ K. The estimated H_2 column densities are $\sim 1 \times 10^{19} \text{ cm}^{-2}$ (IGR J16318–4848) and $5 \times 10^{18} \text{ cm}^{-2}$ (GX 301–2). This implies that the optical extinction associated with the warm molecular gas is very small, $A_V \ll 1$, based on the relation $N_{\text{H}} = 1.87 \times 10^{21} A_V$ (Draine 2003).

5. Discussion and Conclusion

Our *SPITZER* spectroscopic observations of IGR J16318–4848 and GX 301–2 have revealed for the first time the rich mid-IR environment of highly-obscured X-ray binaries. This includes two dust components with prominent silicate absorption, numerous H I recombination lines, many forbidden ionic lines, and pure rotational H_2 lines. Based on the observed spectra, we infer the following components for IGR J16318–4848 and GX 301–2: (1) hot ($T > 700$ K) and warm ($T \sim 180$ K) circumstellar dust; (2) ionized stellar winds responsible for the H I lines; (3) extended low-density ionized regions for the forbidden lines; and (4) photo-dissociated regions associated with the PAH, H_2 and possibly the [Si II] line emission. For the forbidden lines, all the detected lines have relatively low ionization potentials like in starburst galaxies where the radiation is relatively soft (compared with active galactic nuclei, for instance). This may indicate that the illumination of hard X-rays from the central compact X-ray source is not primarily responsible for the forbidden line emission. However, the inferred temperature for the radiation exciting the [Ne II] and [Ne III] lines is hotter than the stellar photospheres, so there can be some contribution from the compact object. Considering that [Ni II] and [Fe II] were detected only in IGR J16318–4848 while [Fe III] was only in GX 301–2, the radiation field of IGR J16318–4848 may be softer than GX 301–2, as demonstrated by the small temperature difference between the two sources (see § 4).

Perhaps the most natural explanation for the origin of the hot dust component relies on dust formation in the dense outflows from the early-type companions of IGR J16318–4848 and GX 301–2, as is the case in most sgB[e] stars (i.e., B-type supergiants with forbidden emission lines). However, the origin of the warm circumstellar dust component is very uncertain, and B[e] stars seldom show evidence for this type of warm dust. If both the hot and warm dust components have spherical shell geometries around the central star, then the associated optical extinctions are: $A_V \simeq 4 \times 10^{-4} Q_{\text{abs}} (M_{\text{d}}/10^{-6} M_{\odot}) (T_{\text{d}}/100 \text{ K})^4 (L_{\text{UV}}/10^{39} \text{ ergs s}^{-1})$, where M_{d} and T_{d} are the mass and temperature of the dust components, $Q_{\text{abs}} < 1$ is the dust absorption coefficient, and L_{UV} is the ultra-violet luminosity of the central star.

This gives the optical extinctions $A_V \ll 1$ for both the hot and warm dust components of IGR J16318–4848 and GX 301–2. (Here we use 1×10^{39} ergs s $^{-1}$ for L_{UV} for both sources.) Therefore, under the assumption of spherical shell geometry, both the hot and warm dust components of IGR J16318–4848 and GX 301–2 contribute very little to the total optical extinction, suggesting that the hot and warm dust components are *NOT* strongly associated with the silicate absorption features. This also applies to the dust associated with the warm extended H $_2$ gas since the optical extinction from this component is tiny (i.e., $A_V \ll 1$; see § 4). What’s then the origin of the silicate absorption features? If it is due to the foreground ISM, we would expect to see the CO $_2$ ice feature around 15 μ m, especially for IGR J16318–4848, based on the intensity ratio between the silicate absorption feature and ice feature found in the ISM (Knez et al. 2005). The absence of the ice feature in our spectra supports the interpretation that the silicate absorption features are probably not associated with the foreground ISM. One possibility may be the existence of an undisclosed colder (e.g., $\ll 100$ K) circumstellar dust component which is responsible for the silicate absorption features and most of the optical extinction. We need further longer wavelength observations to confirm this possibility. Considering that the 9.7 μ m silicate absorption feature represents the oxygen-rich material, the existence of the 9.7 micron silicate absorption feature may indicate that the origin of the potential colder dust component is related to the nucleosynthesis of the progenitors of IGR J16318–4848 and GX 301–2 (or their companions).

The optical/near-IR companion of IGR J16318–4848 is a sgB[e] star. Such stars are known to have hot ($T \sim 1000$ K) circumstellar dust, and probably are evolving into Luminous Blue Variables (LBVs) or Wolf-Rayet stars. Our mid-IR spectra of IGR J16318–4848 and GX 301–2 are very similar to that of the LBV P Cygni which shows many H I lines and forbidden ionic lines (Lamers et al. 1996b). The difference is that while the mid-IR continuum of P Cygni is due to the free-free emission in stellar winds, the main mid-IR emission of IGR J16318–4848 and GX 301–2 is from multiple dust continua. (The SEDs of both sources observed here are inconsistent with the free-free emission, as mentioned in Paper I.) However, we note that some LBV stars have also been observed to have thermal mid-IR dust emission (Lamers et al. 1996a). Based on the fact that B[e] stars seldom show mid-IR forbidden line emission, the B-type supergiant (or hypergiant) companions of IGR J16318–4848 and GX 301–2 may be in the evolutionary track to LBVs, implying that the extremely high obscuration seen in some massive X-ray binaries may be a phenomenon associated with the evolutionary phase. This scenario is also consistent with the fact that the highly-obscured massive X-ray binary Cygnus X-3 has a Wolf-Rayet star companion, together with the circumstellar dust emission of $T \sim 250$ K (Koch-Miramond et al. 2002).

This work is based on observations made with the Spitzer Space Telescope, which is

operated by the Jet Propulsion Laboratory, California Institute of Technology, under a contract with NASA. D.-S.M thanks Elise Furlan for her help in IRS data analysis and Marten van Kerkwijk for comments. This research was partly supported by the Discovery Grant (327277) of Natural Science and Engineering Research Council of Canada to D.-S.M.

REFERENCES

- Alexander, T., Sturm, E., Lutz, D., Sternberg, A., Netzer, H., & Genzel, R. 1999, *ApJ*, 512, 204
- Bodaghee, A., et al. 2007, *A&A*, accepted (astro-ph/0703043)
- Chiar, J. E., et al. 2007, *ApJ*, 666, L73
- Courvoisier, T. J.-L., et al. 2003, *IAU Circ.*, 8063, 3
- Filliatre, P., & Chaty, S. *ApJ*, 616, 469
- Draine, B. T. 2003, *ARA&A*, 41, 241
- Hildebrand, R. H., et al. 2004, *ApJS*, 154, 18
- Houck, J. R., Shure, M. A., Gull, G. E., & Herter, T. 1984, *ApJ*, 287, L11
- Houck, J. R., et al. 2004, *ApJS*, 154, 18
- Hummer, D. G., & Storey, P. J. 1987, *MNRAS*, 224, 801
- Kaplan, D. L., Moon, D.-S., & Reach, W. T. 2006, *ApJ*, 649, L107 (Paper I)
- Kaper, L., et al. 1995, *A&A*, 300, 446
- Koch-Miramond, L., Abraham, P., Fuchs, Y., Bonnet-Bidaud, J.-M., & Claret, A. 2002, *A&A*, 877, 396
- Knez, C., et al. 2005, *ApJ*, 635, L145
- Kunze, D., et al. 1996, *A&A*, 315, L101
- Lamers, H. J. G. L. M., et al. 1996a, *A&A*, 315, L225
- Lamers, H. J. G. L. M., et al. 1996b, *A&A*, 315, L229

- Mathis, J. S. 2000, in *Allen’s Astrophysical Quantities*, ed. A. N. Cox (London: Athlone Press, Ltd.), 527
- Revnivtsev, M. G., Sazonov, S. Yu., Gilfanov, M. R., & Sunyaev, R. A. 2003, *Astron. Lett.*, 29, 587
- Walter, R., et al. 2003, *A&A*, 411, L427
- Werner, M. W., et al. 2004, *ApJS*, 154, 1
- Winkler, C., et al. 2003, *A&A*, 411, L349

Table 1. Observed Intensities of H I Transitions

| Transition(μm) | IGR | GX | Transition(μm) | IGR | GX |
|-----------------------------|--------|-------|-----------------------------|--------|-------|
| | J16318 | 301–2 | | J16318 | 301–2 |
| 17–9(10.26) | 4.39 | 2.44 | 12–8(10.50) | 11.57 | 11.40 |
| 16–9(10.80) | 5.60 | 2.20 | 9–7(11.31) | 25.43 | 13.50 |
| 22–10(11.49) | 1.74 | 0.78 | 15–9(11.54) | 6.48 | 1.87 |
| 20–10(12.16) | 2.84 | 1.35 | 7–6(12.37) ^a | 72.02 | 42.12 |
| 18–10(13.19) | 5.15 | 1.70 | 13–9(14.18) | 10.61 | 3.37 |
| 23–11(14.30) | 2.00 | 0.93 | 22–11(14.71) | 5.02 | 0.87 |
| 16–10(14.96) | 5.41 | 1.75 | 20–11(15.82) | 2.79 | 1.33 |
| 10–8(16.21) | 14.66 | 7.32 | 15–10(16.41) | 3.83 | 1.83 |
| 19–11(16.59) | 2.15 | 0.40 | 12–9(16.88) | 7.35 | 3.17 |
| 14–10(18.62) | 4.04 | 1.38 | 16–11(20.92) | 2.69 | 1.14 |
| 9–8(27.80) | 18.71 | 8.86 | ... | ... | ... |

Note. — The values are in 10^{-14} ergs s^{−1} cm^{−2} and are not corrected for extinction.

^aThe H I 11–8 transitions may be blended.

Table 2. Observed Intensities of Other Lines

| Line(μm) | IGR J16318 | GX 301–2 | Line(μm) | IGR J16318 | GX 301–2 |
|---------------------------------|---------------|-------------|---------------------------------|---------------|-------------|
| [Ni II](10.68) | 10.25 | ... | [Ni II](12.73) | 13.33 | ... |
| [Ni II](18.24) | 1.69 | ... | ... | ... | ... |
| [Ne II](12.81) | 21.44 | 23.41 | [Ne III](15.56) | 2.60 | 15.67 |
| [Fe II](17.94) | 22.54 | ... | [Fe II](24.52) | 7.33 | ... |
| [Fe II](25.99) | 70.93 | ... | [Fe II](35.35) | 15.46 | ... |
| [Fe III](22.93) | ... | 1.99 | ... | ... | ... |
| [S III](18.71) | 7.73 | 8.02 | [S III](33.48) | 40.14 | 25.01 |
| [Si II](34.82) | 177.20 | 33.33 | ... | ... | ... |
| H ₂ (0,0)S(2)(12.28) | 2.88 | 1.44 | H ₂ (0,0)S(1)(17.03) | 4.66 | 2.05 |
| H ₂ (0,0)S(0)(28.22) | 10.08 | 4.24 | ... | ... | ... |

Note. — The values are in 10^{-14} ergs s⁻¹ cm⁻² and are not corrected for extinction.

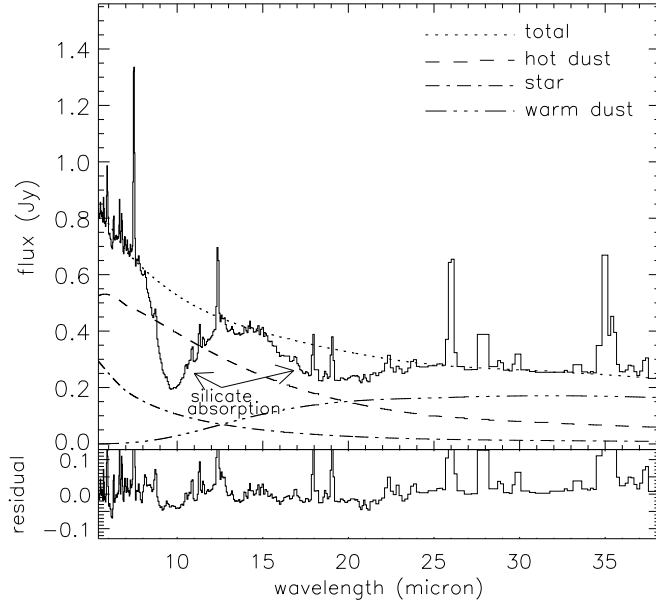


Fig. 1.— *Main Panel:* The background-subtracted IRS low-resolution spectrum of IGR J16318–4848. The solid line represents the observed spectrum, while the dotted line shows the best-fit spectrum combining the hot dust (dashed line), the stellar (dotted-dashed line), and the warm dust (dot-dashed line) components. The SED fit was conducted excluding the wavelengths associated with the silicate absorption features indicated by the arrows around 9.7 and 18 μm . *Bottom Panel:* The residuals of the SED fits. Note that for the residual the fluxes of the wavelengths associated with the silicate absorption features were calculated with the best-fit parameters (see text). The unit of the residual is Jy.

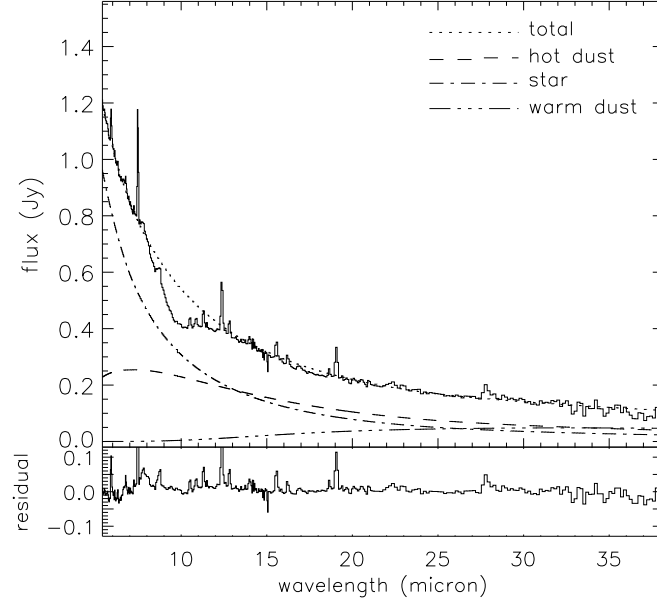


Fig. 2.— Same as Figure 1, but for GX 301-2. The silicate absorption features are not as prominent as in IGR J16318-4848, but are still visible, especially around $\sim 9.7 \mu\text{m}$.

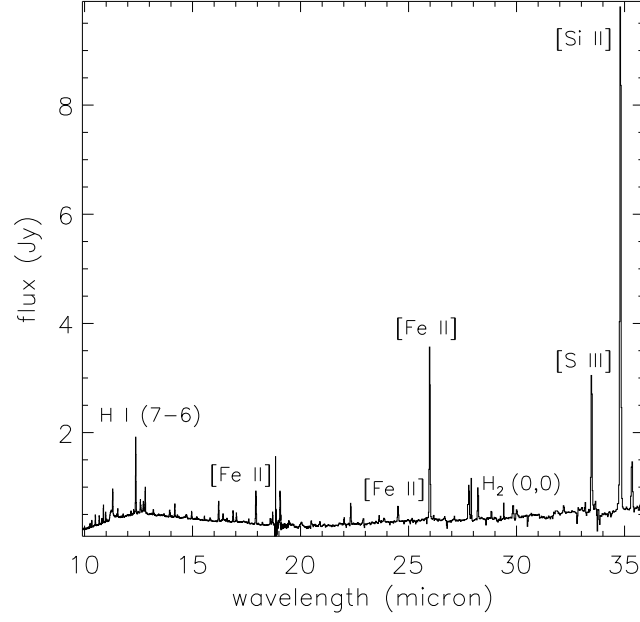


Fig. 3.— The IRS high-resolution spectrum of IGR J16318–4848. Note that the background is *NOT* subtracted. Some strong lines are marked.

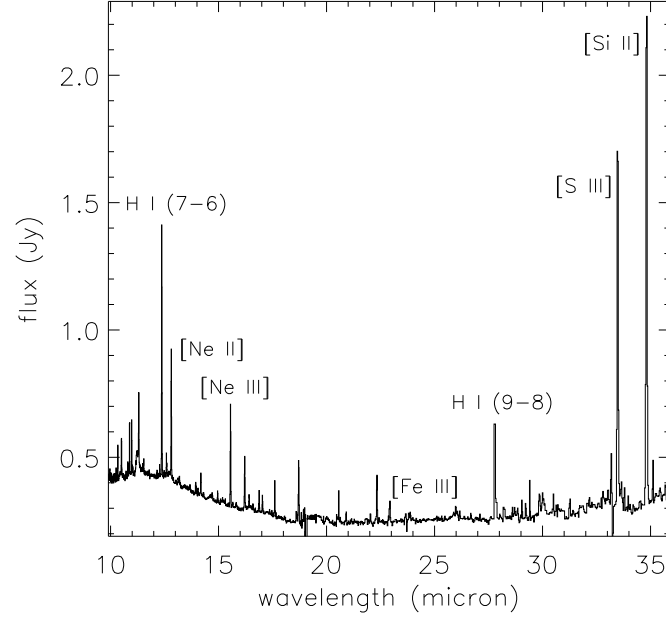


Fig. 4.— Same as Figure 3, but for GX 301-2.